COMPARATIVE GEOCHEMICAL XRF ANALYSIS OF ROCKS FROM IRATI FORMATION, PARANA SEDIMENTARY BASIN, BRAZIL

[1]GABRIELLE ROVERATTI, [2]DANIEL MARCOS BONOTTO

PPGGMA-IGCE, Universidade Estadual Paulista (UNESP), PRH-40.1,
UNESP - Universidade Estadual Paulista UNESP
E-mail: gabrielle.roveratti@unesp.br, daniel.bonotto@unesp.br

This study presents a comparative geochemical evaluation of the Irati Formation, Paraná Sedimentary Basin (Brazil), using X-ray fluorescence (XRF) for major and trace oxides characterization. Twenty rock samples were analyzed with two wavelength-dispersive XRF spectrometers (S8 Tiger, Bruker) located at the Instituto Senai de Inovação (São Bernardo do Campo, SP) and at LARIN/UNESP (Rio Claro, SP). Statistical treatments, including Pearson's correlation, mean percent difference, paired t-test, and p-value assessments, were applied using Python-based libraries. Results indicate strong correlations for most oxides, notably SiO_2 ($r = 0.92$, $p = 0.0001$), P_2O_5 ($r = 0.94$, $p = 0.0001$), and CaO ($r = 0.90$, $p = 0.0001$), reflecting consistency between the instruments. However, certain oxides, such as SrO ($r = 0.16$, $p = 0.5004$) and CuO ($r = 0.39$, $p = 0.0891$), showed weak or non-significant correlations, pointing to potential analytical differences. The combination of high reproducibility for major oxides with observed variations in specific elements highlights both the reliability and the limitations of inter-instrument comparisons. Overall, these findings strengthen the understanding of the geochemical composition of the Irati Formation and contribute to its assessment as a hydrocarbon-bearing sequence within the Paraná Basin.

Keywords - X-ray fluorescence (XRF), Irati Formation, Geochemistry , Paraná Sedimentary Basin.

I. INTRODUCTION

Wilhelm C. Röntgen, a physicist, discovered X-rays in 1895 through an experiment that scientist Max von Laue later confirmed and supplemented [1- 2].

The foundation of instrumental multi-element analysis by X-ray fluorescence (XRF) is the measurement of the intensity of distinctive X-rays released by chemical elements in a sample when appropriately excited. Only wavelength-dispersive spectrometers (WD-XRF), which adhere to Bragg's rule and necessitate precisely coordinated movement between the diffracting crystal and the detector, were used for XRF prior to 1966 [3].

The relative simplicity of X-ray fluorescence (XRF) in assessing sample components is one of its primary benefits. Other procedures that call for costly, time-consuming, and dangerous sample preparation methods are ICP and AAS. XRF, on the other hand, may examine every component directly without destroying the sample entirely. XRF provides a simple way to measure almost any kind of solid or liquid [4]. Because it allows for the simultaneous or sequential measurement of several element concentrations without destroying the sample—that is, without the introduction of chemical precursors—this method is primarily used on solid samples. Liquid samples may be subjected to chelation, precipitation, ion exchange, pre-concentration, and other techniques.
The method offers high analytical speed for semi-quantitative examinations of environmental, geological, and agro-industrial samples when excited by an X-ray tube. Furthermore, during excitation, low-energy radioactive X-ray and gamma-ray generating sources (^{55}Fe, ^{57}Co, ^{109}Cd, ^{238}Pu, and ^{241}Am) have been used in place of X-ray tubes. This method has the disadvantage of losing analytical sensitivity even though it streamlines the study and lowers expenses [5].

However, there are several uses for energy-dispersive XRF (ED-XRF) with radioactive source excitation, especially in geological, industrial, and mineral exploration domains where analytical sensitivity is not a constraint. A variation of energy-dispersive XRF, total reflection X-ray fluorescence (TXRF), has grown dramatically in the last several years. It is mainly used for the analysis of trace elements (ppb level) in liquid samples (microliter volumes) in studies pertaining to oceanography, biology, medicine, industry, mineralogy, and environmental monitoring. It is particularly used for the analysis of biological fluids, groundwater, surface waters (rain, rivers, and seas), and even for quality control of high-purity products.

TXRF can also be applied to solid materials (soil, sediments, air filters, particulate matter, etc.), though this requires prior chemical digestion and proper dilution, as used in flame photometry, spectroscopy, and atomic absorption/emission techniques (AES) and their variants (ICP/AES, ICP/MS). For this type of sample, TXRF offers the advantage of requiring only small amounts (milligrams) for digestion [6].

The global energy matrix still relies heavily on oil, despite the constant hunt for alternative energy sources. Therefore, the need for novel materials extends beyond bettering extraction and refining; it

also includes recycling carbon dioxide (CO_2) and other molecules created from the usage of fossil fuels and using them more efficiently [7]. In Brazil's Paraná Sedimentary Basin (PSB), the Irati Formation is regarded as one of the primary sequences that produce hydrocarbon products in it.

It is made up of sediments that are rich in organic matter, primarily carbonates and shales, which produce oil. This formation is considered immature under typical burial conditions, although it can become mature when igneous intrusions alter its temperature. With correlations to all known oil accumulations, both at the surface and subsurface, geochemical studies have shown that the Irati Formation is the most promising oil-bearing sequence in the area [8].

In this study, XRF is applied to the geochemical characterization of the Irati Formation, supporting the understanding of its compositional features and their implications for hydrocarbon potential.

II. MATERIALS AND METHODS

The research area is situated in the city of Saltinho, State of São Paulo, Brazil, which is located on the Cornélio Pires highway (SP-127), Km 57, in the municipality of Saltinho (SP) (Figure 1), with access via the Cornélio Pires Highway, BR-373. The study area is the Monte Olimpo Pit of Mineradora Amaral Machado (Figure 2), geologically inserted in the PSB, with the rock samples being collected in an outcrop named Pam 19. The rock samples analysis by XRF followed the analytical protocol described by [9]: the samples were ground to approximately <74 µm in a Herzog mill, model HSM 100P-MA15277-5-1. The resulting powder (~8 g) is mixed with Oregon CAS9002-88-4 wax (~1.5 g), which serves as a binding agent. Soon after, boric acid is added to the press, and this mixture is pressed, resulting in a pellet that is then inserted into the spectrometer.

The 20 samples used in this study were analyzed using the S8 Tiger spectrometer from Bruker Co., located at the *Instituto Senai de Inovação*, São Bernardo do Campo (SP), Brazil, as well as a similar spectrometer installed at LARIN-Laboratory of Ionizing Radiations, UNESP, Rio Claro (SP), Brazil.

To ensure analytical accuracy and reproducibility, the samples were first homogenized, finely grounded, and compacted into pressed powder pellets (Figure 4) [9, 10]. The analytical principle of XRF is based on the interaction of incident X-rays with the atoms in the sample, promoting the excitation of inner-shell electrons and the subsequent emission of element-specific secondary radiation (Figure 3) [11]. These analyses were carried out using a Bruker S8 Tiger wavelength-dispersive XRF spectrometer (Figure 5) [10].

The results were subsequently subjected to statistical treatments performed in Python. For descriptive statistical analysis and exploratory graphical representations, the data were processed using the Python programming language [12] and associated libraries such as pandas, numpy, and matplotlib [12]–[14].

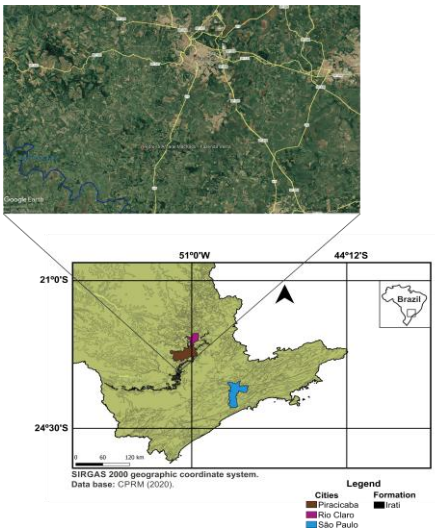

Figure 1- Rock sampling points.

A comparative analysis was conducted for all samples in order to assess reproducibility, since both instruments are of the same model and manufacturer.

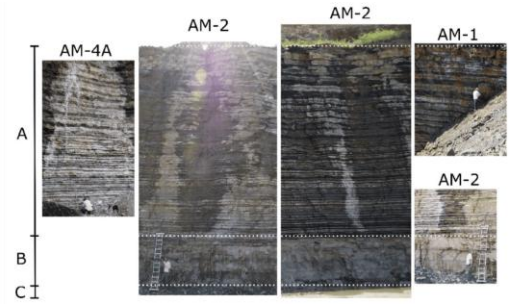

Figure 2 - Studied outcrop [15] and images provided by Mitsuru Arai.

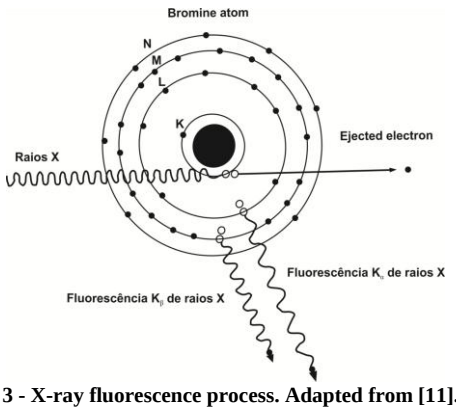

Figure 3 - X-ray fluorescence process. Adapted from [11].



Figure 4 - Preparation of pressed powder pellets for XRF analysis. Samples were homogenized, grounded, and compacted into pellets under controlled pressure to ensure analytical reproducibility.

III. RESULTS AND DISCUSSION

Table 1 shows the results obtained for all readings. Table 2 summarizes the results obtained for the Pearson Correlation, Mean Percent Difference, p-value Test, Standard Deviation, and paired t-test, considering the readings of both spectrometers. Based on the literature, as noted by [16], the paired t-test is used to compare two means in related measurements, such as laboratory analyses performed on different instruments.

In addition, Pearson's correlation is commonly employed to evaluate the linear relationship between values obtained by different methods [17]. The Pearson correlation coefficient (r) ranges from -1 to +1, with values close to -1 and +1 indicating strong linear correlation, while values near 0 indicate the absence of a linear relationship. These results are summarized in Table 2.



Figure 5 - Bruker S8 Tiger wavelength-dispersive X-ray fluorescence (WDXRF) spectrometer used for geochemical analyses located at LARIN/UNESP (Rio Claro, SP).

Based on the results obtained, the following features can be drawn:

• **Pearson Correlation (Table 2):** The results show that most oxides exhibit a high correlation between data from the two instruments ($r > 0.7$), suggesting consistency in the trends of the values, even though absolute variations occur. Notably, SiO_2 ($r = 0.92$), CaO ($r = 0.89$), and P_2O_5 ($r = 0.89$) display very strong correlations, indicating similar readings in both instruments. Conversely, SrO ($r = 0.16$) and CuO ($r = 0.30$) show weak correlations, suggesting differences between the instruments readings for these oxides.

• **Paired t-test and Percent Differences:** The t-test indicated statistically significant differences ($p < 0.05$) for most oxides, including Fe_2O_3, MgO, Na_2O, MnO, and CuO. This suggests that although the data are correlated, there is a real difference in the means obtained between the methods. For example, Fe_2O_3 showed a mean percent difference of -46.05% with $p = 0.0001$, pointing out to a significant difference of large relative magnitude. In contrast, Al_2O_3 showed a mean difference of only 16.44% with $p = 0.8478$, which was not statistically significant.

• **Validity and Reliability Between Instruments:** Despite the high correlation observed for several

oxides, the mean percent differences and t-tests indicate that absolute values are not directly interchangeable. This discrepancy may be attributed to calibration issues, operation mode or the application of correction factors. The spectrometer installed at LARIN is devoted chiefly for analyzing rocks, minerals, and sediments, with the following standards being utilized for calibration: cement, clay, feldspar, limestone, dolomite, sediment, sillimanite, magnesite, refractory, carbonatite, silica, bauxite, gypsum, superphosphate and five additional rock types [18]. The concentration range (in %) of the major constituents in the standards corresponded to: SiO_2 (0.712 – 99.880), Al_2O_3 (0.036 – 90.800), TiO_2 (0.010 – 7.794), Fe_2O_3 (0.012 – 39.078), Mn_3O_4 (0.007 – 0.789), CaO (0.006 – 97.880), MgO (0.015 – 95.769), Na_2O (0.020 – 11.301), K_2O (0.005 – 15.364), P_2O_5 (0.008 – 19.340), and SO_3 (0.019 – 54.38) [18]. On the other hand, the equipment installed at Senai is also dedicated for analysis of other materials, such as steel, alloys, concrete, etc., which demand different analytical protocols for data acquisition.

Based on Pearson's correlation coefficient (r), the p-value was obtained to assess whether r is statistically significant. Traditionally, the cutoff value for rejecting the null hypothesis is 0.05, meaning that when no difference exists, such an extreme value for the statistical test would be expected in less than 5% of cases [19]. Table 3 presents the p-values for the data obtained, classified as not significant ($p \geq 0.1$), marginally significant ($p \geq 0.05$), and statistically significant ($p < 0.05$). The free software GraphPad was used, considering 18 degrees of freedom. Figure 6 plots the relationships among the oxides analyzed by both spectrometers. It is possible verify the significant correlations in the readings obtained for several oxides, for instance, r = 0.92 for SiO_2; r = 0.67 for MgO; r = 0.71 for Fe_2O_3; etc.

The statistical evaluation of the major oxides revealed that most oxides exhibited strong and highly significant correlations considering the readings of both instruments. In particular, SiO_2 (r = 0.92, p = 0.0001), Al_2O_3 (r = 0.80, p = 0.0001), CaO (r = 0.90, p = 0.0001), TiO_2 (r = 0.87, p = 0.0001), and P_2O_5 (r = 0.94, p = 0.0001) demonstrated extremely significant relationships, indicating strong consistency in the readings.

Other oxides, such as MgO, Fe_2O_3, K_2O, Na_2O, and MnO, also presented extremely significant correlations ($r > 0.67$, $p < 0.001$), reinforcing the reproducibility of the analytical results. SO_3 showed a moderate but statistically significant correlation (r = 0.51, p = 0.0216). In contrast, SrO (r = 0.16, p = 0.5004) and CuO (r = 0.39, p = 0.0891) did not reach statistical significance, as already pointed out. Overall, the results confirm the robustness of the measurements for most major oxides while highlighting specific cases where reproducibility between instruments is limited.

Other significant correlations were found among oxides such as Fe_2O_3–SiO_2, SO_3–SiO_2, Al_2O_3–SiO_2, Na_2O–SiO_2, and TiO_2–SiO_2, in both instruments. Two correlations, K_2O–Al_2O_3 and TiO_2–SiO_2, with respective values of 0.99 and 0.91, were observed in the measurements obtained from the instrument located at the Senai. Significant inverse correlations were also identified, for example, MgO–SiO_2, SiO_2–CaO, and Fe_2O_3–CaO. It is important to emphasize that, in general, the reading trends for the oxides are consistent across both instruments, with values

Oxide	Mean (%)	Median (%)	Std. Dev. (%)	Min (%)	Max (%)	N
SenaiSiO_2	41.97	41.47	15.21	9.30	63.77	20
LarinSiO_2	45.84	48.02	14.06	13.36	67.23	20
SenaiMgO	16.85	18.49	5.00	5.51	25.96	20
LarinMgO	23.87	23.69	7.85	8.33	41.21	20
SenaiFe_2O_3	5.64	5.39	2.85	0.53	9.98	20
LarinFe_2O_3	3.30	2.71	2.69	0.13	8.70	20
SenaiSO_3	3.60	2.70	2.64	0.40	9.31	20
LarinSO_3	2.73	2.11	2.00	0.30	7.04	20
SenaiAl_2O_3	4.34	3.34	2.90	0.64	10.04	20
LarinAl_2O_3	4.41	3.50	2.73	1.08	9.42	20
SenaiCaO	2.84	20.90	18.10	1.28	60.93	20
LarinCaO	17.21	15.12	14.86	0.77	57.32	20
SenaiK_2O	1.08	0.65	0.96	0.07	3.01	20
LarinK_2O	0.74	0.40	0.76	0.09	2.70	20
SenaiNa_2O	0.83	0.88	0.35	0.23	1.47	20
LarinNa_2O	1.12	1.08	0.50	0.26	2.11	19
SenaiTiO_2	0.35	0.27	0.25	0.03	0.77	20
LarinTiO_2	0.24	0.15	0.21	0.03	0.70	18
SenaiP_2O_5	0.14	0.12	0.07	0.07	0.40	19

LarinP_2O_5	0.13	0.11	0.08	0.04	0.41	19
SenaiSrO	0.13	0.12	0.07	0.04	0.31	20
LarinSrO	0.06	0.05	0.05	0.02	0.25	20
SenaiMnO	0.51	0.48	0.41	0.03	1.23	20
LarinMnO	0.26	0.22	0.27	0.02	1.02	20
SenaiBaO	0.069	0.07	0.0179	0.04	0.1	10
LarinBaO	0.15	0.12	0.1052	0.06	0.3	4
SenaiZrO_2	0.0483	0.055	0.0194	0.02	0.07	6
LarinZrO_2	0.0187	0.01	0.016	0.0048	0.06	12
SenaiV_2O_5	0.0244	0.02	0.0088	0.01	0.04	9
Larin V_2O_5	0.0217	0.02	0.0133	0.01	0.04	6
SenaiRb_2O	0.0125	0.01	0.0046	0.01	0.02	8
LarinRb_2O	0.0059	0.0048	0.0035	0.0016	0.01	8
SenaiZnO	0.0111	0.01	0.0033	0.01	0.02	9
LarinZnO	0.0078	0.0056	0.006	0.0022	0.02	12
SenaiCl	0.0431	0.04	0.0193	0.01	0.07	13
LarinCl	0.0364	0.04	0.0145	0.01	0.06	14
SenaiZrO_2	0.02	0.02		0.02	0.02	1
LarinZrO_2	0.0127	0.0096	0.0085	0.0081	0.03	6
SenaiCr_2O_3	0.01	0.01	0	0.01	0.01	2
LarinCr_2O_3	0.0062	0.0062		0.0062	0.0062	1
SenaiCuO	0.0133	0.01	0.0049	0.01	0.02	18
LarinCuO	0.0061	0.0049	0.0049	0.0022	0.02	13

Table 1 - Statistics for the XRF readings. N=used samples.

Oxide	N	N2	r	P_r Value	MPD (%)	SDD	t	P_t value
SiO_2	20	0	0.92	0.0001	17.19	5.93	-2.843	0.0104
MgO	20	0	0.67	0.0012	50.03	5.673	-5.393	0.0001
Fe_2O_3	20	0	0.71	0.0004	-46.05	2.048	4.967	0.0001
SO_3	20	0	0.83	0.0001	-18.02	1.452	2.606	0.0174
Al_2O_3	20	0	0.80	0.0001	16.44	1.748	-0.195	0.8478
CaO	20	0	0.89	0.0001	23.23	7.983	2.528	0.0205
K_2O	20	0	0.74	0.0002	-24.73	0.633	2.322	0.0315
Na_2O	19	1	0.72	0.0003	46.59	0.326	-3.855	0.0011
TiO_2	18	2	0.77	0.0001	-22.09	0.152	3.301	0.0038
P_2O_5	18	2	0.89	0.0001	-5.85	0.034	1.272	0.2188
SrO	20	0	0.16	0.492	-42.96	0.075	3.739	0.0014
MnO	20	0	0.74	0.0002	-36.33	0.273	3.872	0.001
CuO	11	9	0.30	0.2035	-52.26	0.005	6.419	0.0001

Table 2 - Statistics summarizing the readings obtained by both XRF spectrometers.

NOTE: N=valid pairs; N2=discarded pairs; r=Pearson correlation; P_r value = from Pearson; MPD=Mean percentage difference (%); SDD=Standard deviation of differences; t=t (paired test); p_t= p-value t.

Correlation	r Value	p value	Classification
SiO_2	0.92	0.0001	Extremely significant
MgO	0.67	0.0012	Extremely significant
Fe_2O_3	0.71	0.0005	Extremely significant
SO_3	0.51	0.0216	Significant
Al_2O_3	0.80	0.0001	Extremely significant
CaO	0.90	0.0001	Extremely significant
K_2O	0.74	0.0002	Extremely significant
Na_2O	0.72	0.0003	Extremely significant
TiO_2	0.87	0.0001	Extremely significant
P_2O_5	0.94	0.0001	Extremely significant
SrO	0.16	0.5004	Not significant

MnO	0.74	0.0002	Extremely significant
CuO	0.39	0.0891	Not significant

Table 3 - P-values and significance ratings obtained for the major oxides.

being close. Figure 7 summarizes these relationships. The free software GraphPad was used, considering 18 degrees of freedom.

The correlation analysis revealed distinct patterns between the two spectrometers. In the SENAI dataset, strong negative correlations such as SiO_2–CaO and Al_2O_3–CaO reflect the mineralogical balance between silicate and carbonate phases, a relationship commonly reported in sedimentary and igneous systems [20, 21].

Conversely, the LARIN dataset emphasizes positive correlations such as Fe_2O_3–TiO_2 and Al_2O_3–TiO_2, which are

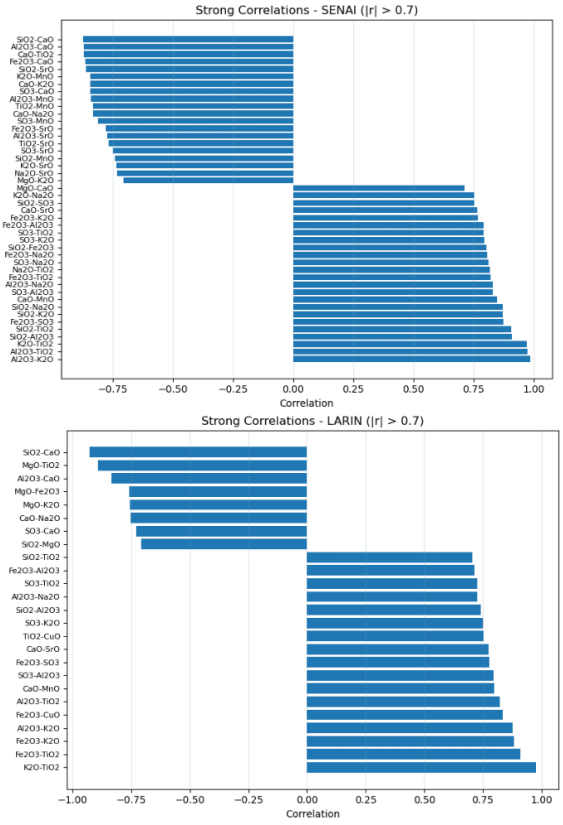

Figure 7 - Strong correlations between oxides analyzed by both equipment.

consistent with known geochemical associations between iron oxides, titanite, and aluminosilicates [20].

In general, data generated by the X-ray fluorescence analysis are subjected to several factors like sample preparation, excitation geometry, and matrix effects. As noted by Jenkins and De Vries [22], the spectral overlap of emission lines (particularly for Fe, Ti, and Ca) can introduce systematic deviations if the instrumental corrections are not fully optimized for each matrix. Furthermore, the use of distinct steps of calibration enhances sensitivity to different oxide assemblages, affecting the resulting correlations. Studies by Potts and Webb [23] and Lachance and Claisse [24] have shown that such differences are typical in WDXRF inter-laboratory comparisons, particularly when dealing with materials of variable mineralogy and particle size.

Despite the same types of equipment, differences in the analytical protocols adopted would affect the sensitivity to readings of specific oxides. In this study, the same pressed powder pellets were submitted for readings at both spectrometers. However, the operation mode “Best” (counting time = 14 minutes) was adopted at LARIN, whereas the mode “Fast” (counting time < 2 minutes) provided a semi-quantitative data analysis. This could chiefly imply in the readings of oxides exhibiting low concentration, like SrO and CuO, justifying the differences found.

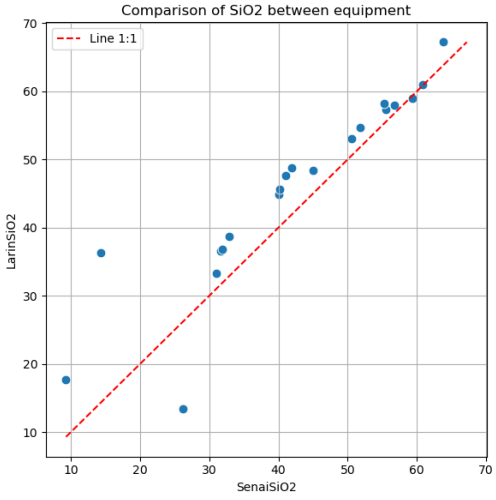

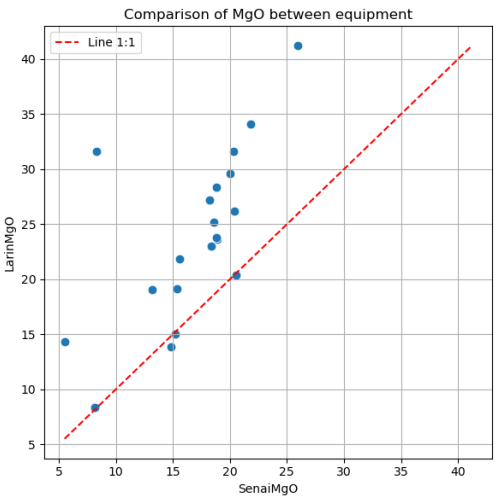

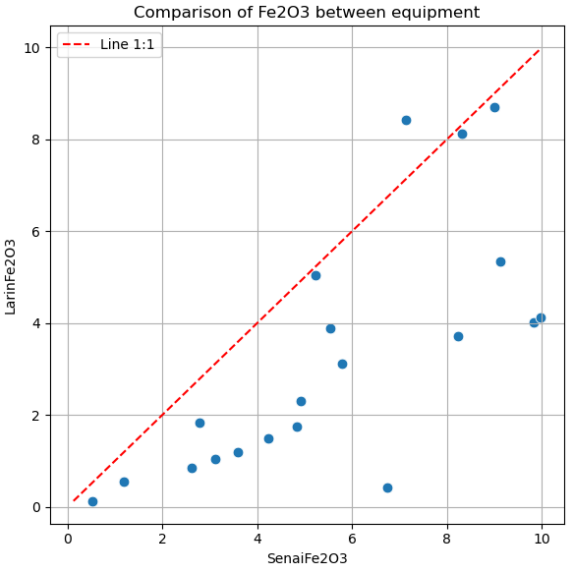
Comparison of Fe2O3 between equipment
Line 1:1
LarinFe2O3
SenaiFe2O3

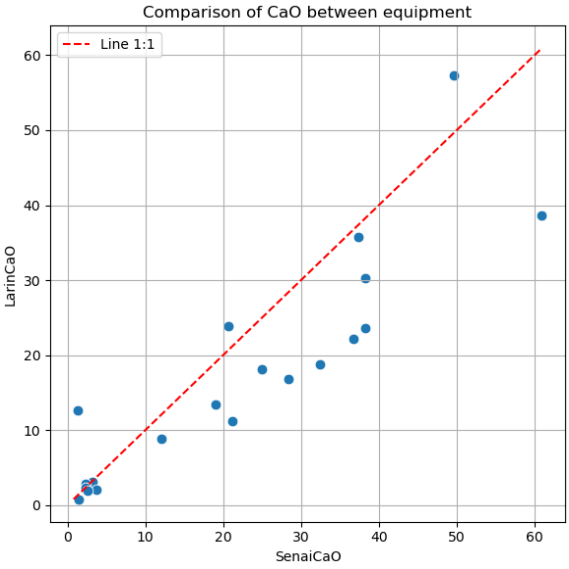
Comparison of CaO between equipment
Line 1:1
LarinCaO
SenaiCaO

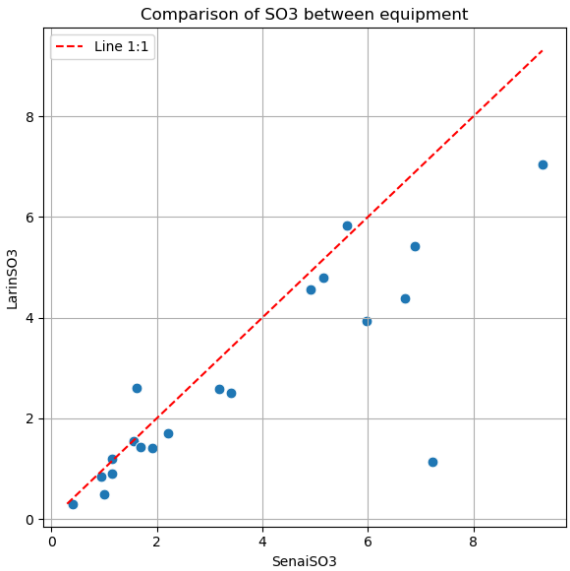
Comparison of SO3 between equipment
Line 1:1
LarinSO3
SenaiSO3

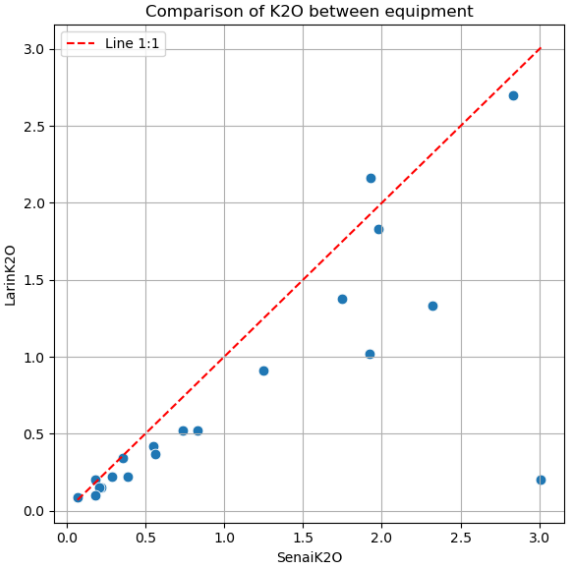
Comparison of K2O between equipment
Line 1:1
LarinK2O
SenaiK2O

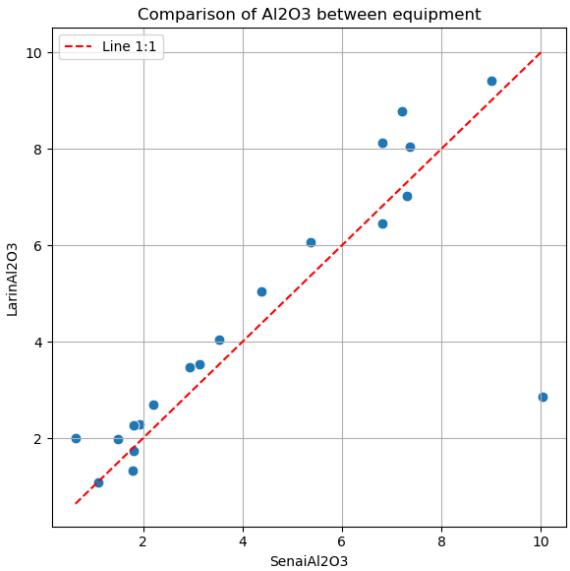
Comparison of Al2O3 between equipment
Line 1:1
LarinAl2O3
SenaiAl2O3

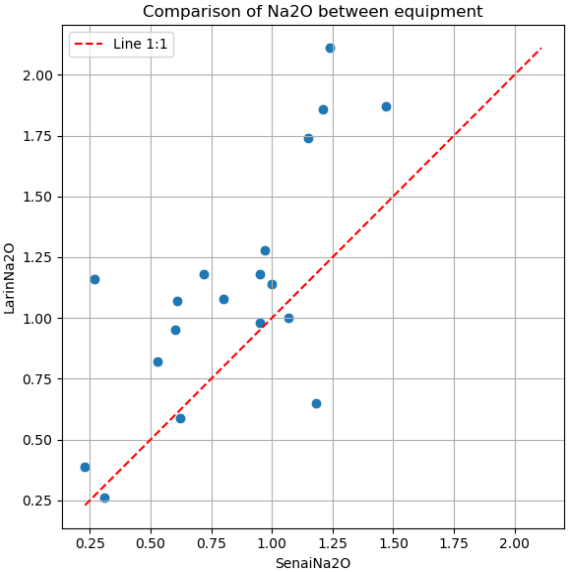
Comparison of Na2O between equipment
Line 1:1
LarinNa2O
SenaiNa2O

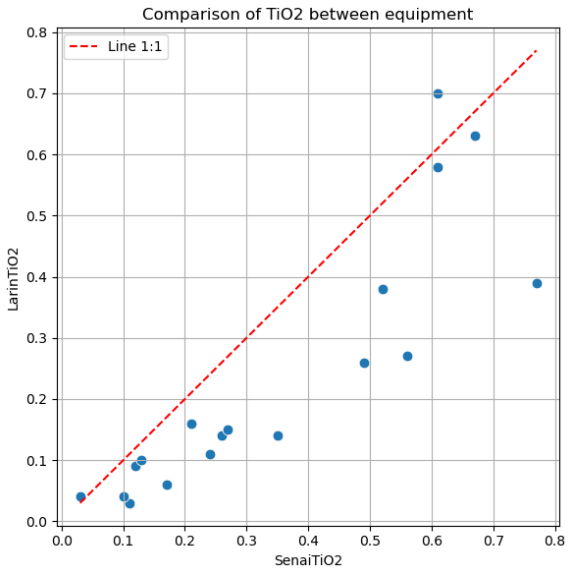

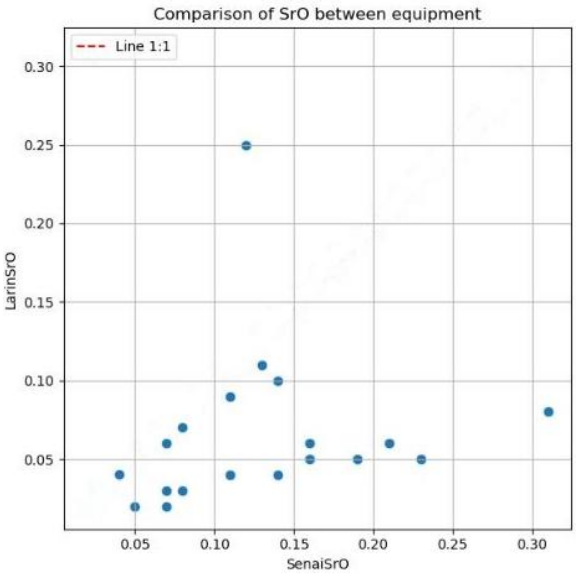

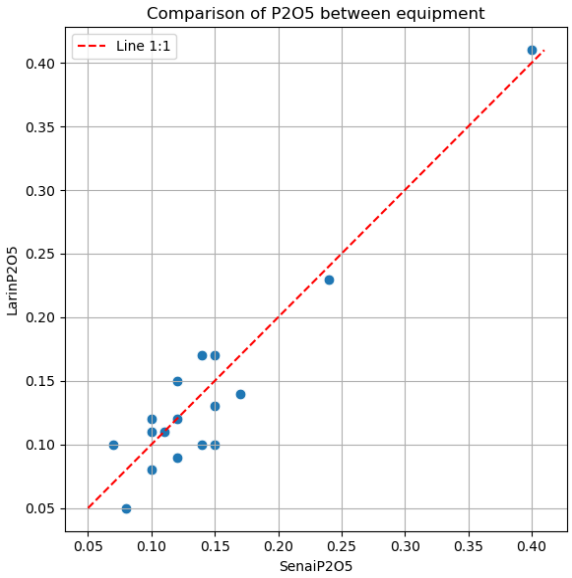

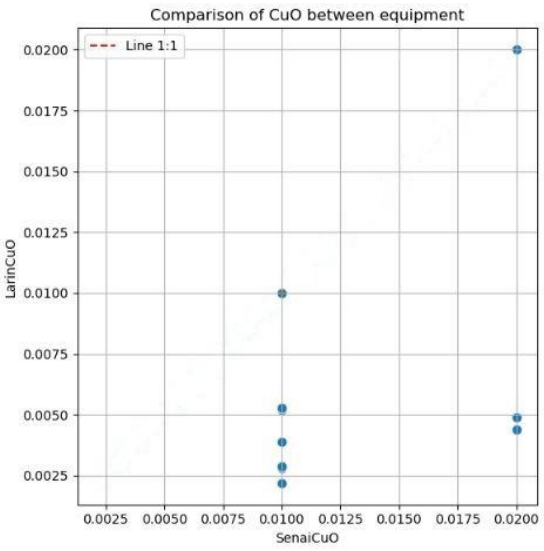

Figure 6 - Comparison of the instruments readings for each oxide.

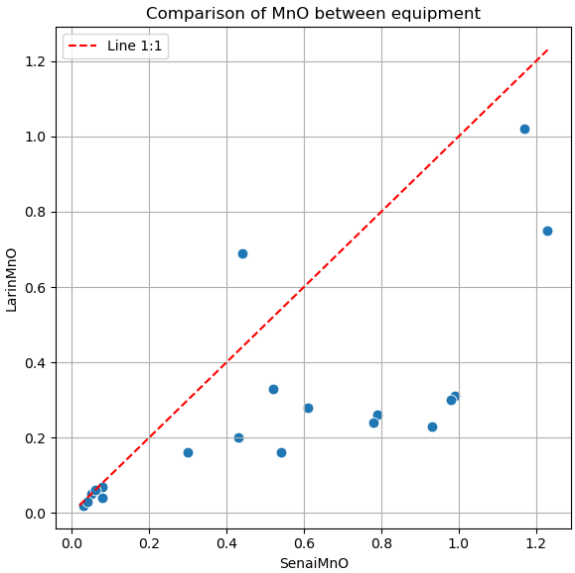

Similar interpretations have been highlighted in statistical treatments of environmental and geochemical data, where instrument-specific effects can alter correlation strengths without compromising overall geochemical trends [21].

Nonetheless, the strong and statistically significant correlations observed for most major oxides confirm the analytical robustness of the Bruker S8 TIGER XRF spectrometer for geochemical analysis of rocks.

IV. CONCLUSIONS

The comparison of XRF data obtained from two identical spectrometers demonstrates that the method provides consistent and reproducible results for most major oxides, validating its application to the geochemical characterization of the Irati Formation. High Pearson correlation values ($r > 0.7$) and

statistically significant results for SiO_2, CaO, P_2O_5, Al_2O_3, and TiO_2 confirm strong agreement between the instruments, despite differences in absolute concentrations. Conversely, the weak correlations and non-significant p-values observed for SrO and CuO indicate that caution must be exercised when interpreting results for these oxides, as they may be influenced by calibration procedures or detection limits. Overall, the study underscores the robustness of XRF as a tool for assessing lithological and compositional features of sedimentary sequences, while also highlighting the need for complementary analyses when dealing with elements of low concentration or analytical sensitivity. These results reinforce the role of XRF in supporting the understanding of hydrocarbon potential and geochemical variability in the Paraná Sedimentary Basin.

REFERENCES

[1] G. W. Brindley, *Quantitative X-ray mineral analysis*. Washington: Mineralogical Society of America, 1980

[2] D. M. Moore and R. C. Reynolds Jr., *X-Ray Diffraction and the Identification and Analysis of Clay Minerals*. Oxford: Oxford Univ. Press, 1989, pp. 179–201.

[3] R. Jenkins, et al., *Quantitative X-ray spectrometry*. New York: Marcel Dekker, 1981, 588 p.

[4] Bruker AXS GmbH, *S8 Tiger Spectrometry Solutions*. Karlsruhe: Bruker AXS GmbH, 2011, pp. 1–31.

[5] IAEA – International Atomic Energy Agency, *Uranium series and radium in the environment*. Vienna: IAEA, 2003.

[6] V. F. N. Filho, "Técnicas analíticas nucleares de fluorescência de raios X por dispersão de energia (ED-XRF) e por reflexão total (TXRF)," Depto de Ciências Exatas/ESALQ, Lab. de Instrumentação Nuclear/CENA, 1999. [Online]. Available: http://www.raiosx.ufc.br/site/wp-content/uploads/downloads/2012/10/EDXRF_TXRF.pdf

[7] C. Koopmann and A. Prange, "Multielement determination in sediments from the German Wadden Sea: investigations on sample preparation techniques," Spectrochim. Acta B, vol. 46, p. 1395, 1991.

[8] LNLS, "A luz síncrotron e seus benefícios." [Online]. Available: https://lnls.cnpem.br/sirius/a-luz-sincrotron-e-seus-beneficios/. [Accessed: Mar. 6, 2024].LNLS. A luz síncrotron e seus benefícios. Disponível em: https://lnls.cnpem.br/sirius/a-luz-sincrotron-e-seus-beneficios/. Acesso em: 06 mar. 2024.

[9] R. V. Santos, et al., "Shrimp U-Pb zircon dating and palynology of bentonitic layers from the Permian Irati Formation, Paraná Basin, Brazil," Gondwana Res., vol. 9, pp. 456–463, 2006.

[10] G. Roveratti and D. M. Bonotto, "End-User Procedure for the Calibration of an X-Rays Fluorescence Spectrometer," in Advances in Chemistry Research, C. James, Ed. New York: Nova Science, 2017, vol. 40, pp. 231–247.

[11] Bruker AXS GmbH, *Introduction to X-ray fluorescence analysis (XRF)*. Karlsruhe: Bruker AXS GmbH, 2010, pp. 1–66.

[12] G. van Rossum and F. L. Drake, *Python 3 Reference Manual*. Scotts Valley: CreateSpace, 2009.

[13] W. McKinney, "Data Structures for Statistical Computing in Python," in Proc. 9th Python in Science Conf., Austin, 2010, pp. 51–56.

[14] J. D. Hunter, "*Matplotlib: A 2D graphics environment*," Comput. Sci. Eng., vol. 9, no. 3, pp. 90–95, 2007.

[15] F. C. Fontes, *Palinoestratigrafia de Alta Resolução do Membro Assistência (Permiano Inferior) na Pedreira Amaral Machado (Saltinho - SP): Contribuição para Estudo de Variação Paleoclimática e Paleoambiental*, Trabalho de Conclusão de Curso (Bacharelado em Geologia), Universidade Estadual Paulista (Unesp), Instituto de Geociências e Ciências Exatas, Rio Claro, 2022.

[16] S. Vieira, *Introdução à bioestatística*, 2nd ed. Rio de Janeiro, Brazil: Elsevier, 2008.

[17] J. C. Ferreira and C. M. Patino, "*What does the p value really mean*?," Jornal Brasileiro de Pneumologia, vol. 41, no. 5, pp. 485–485, 2015. [Online]. Available: https://doi.org/10.1590/S1806-37132015000000215.

[18] Bruker, *Geo-Quant M: Preparation Manual*. Karlsruhe, Germany: Bruker AXS GmbH, 2011, pp. 1–6.

[19] J. C. Ferreira and C. M. Patino, "What does the p value really mean?," Jornal Brasileiro de Pneumologia, vol. 41, no. 5, pp. 485–485, 2015. [Online]. Available: https://doi.org/10.1590/S1806-37132015000000215.

[20] H. Rollinson, Using Geochemical Data: Evaluation, Presentation, Interpretation. Harlow: Longman, 1993.

[21] C. Reimann, P. Filzmoser, and R. G. Garrett, *Statistical Data Analysis Explained: Applied Environmental Statistics with R*. Chichester: Wiley, 2002.

[22] R. Jenkins and J. L. De Vries, *Practical X-ray Spectrometry*, Springer

[23] P. J. Potts and P. C. Webb, "X-ray fluorescence spectrometry," *Journal of Geochemical Exploration*, vol. 44, no. 1–3, pp. 251–296, 1992.

[24] G. R. Lachance and F. Claisse, *Quantitative X-ray Fluorescence Analysis: Theory and Application*, John Wiley & Sons, 1995

★★★